



Characteristics of eco-friendly perovskite solar cell with moth-eye nanostructure array

Afaf Salah Wahba^{1,3} · Ghada Yassin Abdel-Latif² · Shamia El-Sherbiny¹ · Nihal F. F. Areed^{3,4} · Mohamed Farhat O. Hameed^{4,5,6} · S. S. A. Obayya^{3,4}

Received: 15 June 2023 / Accepted: 15 June 2023 / Published online: 23 July 2023
© The Author(s) 2023

Abstract

A novel design of tin perovskite ($\text{CH}_3\text{NH}_3\text{SnI}_3$) solar cell (PSC) is proposed and analyzed for energy harvesting application. The suggested PSC is lead free where moth-eye nanostructures are implemented in the active material to improve the light trapping and hence the light absorption. The suggested SC is numerically studied using finite difference time domain (FDTD) via Lumerical software package. The geometrical parameters and position of the nanostructures are studied to maximize the absorption and hence the optical efficiency. The reported PSC covered by the moth-eye nanostructures exhibits marked light trapping compared to the conventional planar structure with photocurrent density of $46.0082 \text{ (mA/cm}^2\text{)}$, an optical generation rate of $3.38 \text{ e}^{28} \text{ (m}^{-3} \cdot \text{s}^{-1}\text{)}$ and an ultimate efficiency of 31.76% . Therefore, an enhancement of 14.496% is obtained compared to the traditional PSC due to the localized surface plasmons (LSP) modes around the moth eye nanostructures. The suggested design is an efficient replacement to lead—perovskite owing to excellent photovoltaic properties, cheap fabrication cost, suitable band gap of 1.02 eV , eco-friendly and great performance in converting sunlight to electrical energy.

Keywords Eco-friendly perovskite solar cell · Moth-eye nanostructure · Ultimate efficiency

✉ Mohamed Farhat O. Hameed
mfarahat@zewailcity.edu.eg

✉ S. S. A. Obayya
sobayya@zewailcity.edu.eg

¹ Electrical Engineering Department, Faculty of Engineering, Kafr El-Sheikh University, Kafr El-Sheikh, Egypt

² Department of Electronic and Communication Engineering, MISR Higher Institute for Engineering and Technology (MET), Mansoura Ring Road, Mansoura 35516, Egypt

³ Electronics and Communication Engineering Department, Faculty of Engineering, University of Mansoura, Mansoura 35516, Egypt

⁴ Centre for Photonics and Smart Materials, Zewail City of Science, Technology and Innovation, October Gardens, 6Th of October City, Giza 12578, Egypt

⁵ Nanotechnology and Nanoelectronics Engineering Program, Zewail City of Science, Technology and Innovation, October Gardens, 6Th of October City, Giza 12578, Egypt

⁶ Mathematic and Engineering Physics Department, Faculty of Engineering, University of Mansoura, Mansoura 35516, Egypt

1 Introduction

Renewable and sustainable resources of energy have a great attention as efficient alternatives to conventional power sources that are based on fossil fuels (Izadi et al. 2021). In recent years, there have been a great advancement in photovoltaic (PV) technology to produce various solar devices. However, the 3rd generation perovskite solar cells (SCs) have attracted a great interest in scientific world with low-cost implementation and high efficiency (Umari et al. 2014); Liu et al. (2019a). Perovskites have some properties that make them suitable materials for PV solar cells. They have high coefficient of absorption, high mobility carrier, large diffusion length of charge carriers and long carrier life span which lead to a new record of PSC with a good efficiency of 25.2% (Park et al. 2016). They have also a great impact to rebate the manufacturing cost of photovoltaics significantly. The most common type of perovskite materials is [Methylammonium (MA) lead iodide] ($\text{CH}_3\text{NH}_3\text{PbI}_3$) or (MAPbI_3) due to its great performance in PV sector (Hwang et al. 2016); (Burschka et al. 2013). Although these materials have introduced high values of power conversion efficiency (PCE), lead is not eco-friendly (toxic) and harmful to humans and environment. Further, lead-based electronic devices have been harshly restricted by the European union and large number of countries as well. Lead degrades easily when it becomes in contact with water (Huang et al. 2019; Liu et al. 2019a, 2019b). Therefore, lead-free [Methylammonium (MA) tin iodide] ($\text{CH}_3\text{NH}_3\text{SnI}_3$) or (MASnI_3) has been investigated as a PV material due to its outstanding optoelectronic features (Hao et al. 2014a; Hao et al. 2014b; Patel 2021a, 2021b). Additionally, Tin (Sn)—based perovskite is an efficient replacement to lead—perovskite owing to excellent photovoltaic properties, cheap fabrication cost, suitable band gap of 1.02 eV, eco-friendly and great performance in converting sunlight to electrical energy (Poortmans et al. 2006; Nouf et al. 2006).

It has been also proved that the use of Sn doesn't affect badly the performance of the cell. The Sn has a very close chemical similarity to the Pb with improved PCE from 6 to 10%. In addition, tin perovskite (Sn) has been successfully used in SCs since 2014, with low efficiencies within the range from 5.73% to 6.40% (Noel et al. 2014; Hao et al. 2014a, 2014b). Currently, tin perovskite SCs have an efficiency of 14.63%, compared to 25.2% of pb perovskite SC (Jiang et al. 2021). Such an efficiency gap is primarily due to the oxidation of Sn (II) to Sn (IV), low open circuit voltage, poor film quality, and irreproducibility. Although, the efficiency is lower than that of Pb based PSC, there is a room for efficiency enhancement (Jeong et al. 2021). Sunny et al. (2021) have introduced a PSC with layers of FTO/ TiO_2 / $\text{CH}_3\text{NH}_3\text{SnI}_3$ /Ni which produced photocurrent density of 31.93 mA/cm². Patel have achieved photocurrent density of 40.14 mA/cm² (Patel 2021a, b) using FTO/ TiO_2 / $\text{CH}_3\text{NH}_3\text{SnI}_3$ / Cu_2O layers. Additionally, Jayan et al. have demonstrated PSC with 34.27 mA/cm² based on layers of FTO/PCBM/ $\text{CH}_3\text{NH}_3\text{SnI}_3$ /Spiro-OMeTAD/Pd (Jayan et al. 2021). Qasim et al. have suggested a PSC structure using FTO/ZNO/Cds/ $\text{CH}_3\text{NH}_3\text{SnI}_3$ /GaAs/Au layers that offered 33.86 mA/cm² (Qasim et al. 2021). Alam et al. have designed PSC of FTO/ In_2S_3 / $\text{CH}_3\text{NH}_3\text{SnI}_3$ /Spiro-OMeTAD/Au (Alam et al. 2020) which achieved a photocurrent density of 33.44 mA/cm².

Effective light trapping technique can be used to increase the light absorption with improved conversion efficiency (Saffari et al. 2017). In this context, different nanostructures have been used such as cubic (Chen et al. 2021), sphere (Chen et al. 2021; Heidarzadeh et al. 2021), cylinder (Khaled et al. 2021) and cone (Khaled et al. 2021) to improve the absorption of SC. In this paper, thin-film perovskite SC (PSC) is reported and analyzed with Ni moth-eye nanostructures in the active layer. The suggested PSC is lead-free that

consists of layers of ITO, TiO_2 , $\text{CH}_3\text{NH}_3\text{SnI}_3$, and Cu_2O . Further, Ni nanostructures are used to improve the light trapping in the active material with improved optical efficiency. The proposed design is simulated using finite difference time domain (FDTD) method through Lumerical software package (<https://www.lumerical.com/>) to accurately predict the light absorption, photocurrent density and also the generation rate. The suggested PSC achieves photocurrent density of 46.59 mA/cm^2 , generation rate of $5.45 \text{ e}28 \text{ m}^{-3} \cdot \text{s}^{-1}$ and an ultimate efficiency of 33.81% compared to 44.16 mA/cm^2 , $2.07 \text{ e}28 \text{ m}^{-3} \cdot \text{s}^{-1}$ and 29.29% of planar PSC, respectively. The achieved results are better than those presented in (Sunny et al. 2021; Patel 2021a, b; Jayan et al. 2021; Qasim 2021; Alam et al. 2020).

2 Design considerations

Figure 1 shows schematic diagrams of the planar and suggested PSCs with MASnI_3 as an active perovskite material. The planar PSC has an anti-reflection coating glass of indium tin oxide (ITO) (Moerland et al. 2016), and n-type compact layer material of Titanium dioxide (TiO_2) (Guo et al. 2019). The active (absorber) layer has thin film of MASnI_3 perovskite material (Hao et al. 2014a, 2014b); Patel 2021a, 2021b), a p-type layer of copper (I) oxide (Cu_2O) (Khattak et al. 2018; Yu et al. 2015) and back contact layer of Aluminum (Al). Figure 1b shows the proposed PSC with Ni moth-eye nanostructures impeded in the active layer (Soliman et al. 2020a, 2020b). Table 1 shows the geometrical parameters and materials of anti-reflection, absorption, buffer, and protective layers. The ITO anti-reflective coating layer decreases the light reflection and improves its entrance to the PSC. Further,

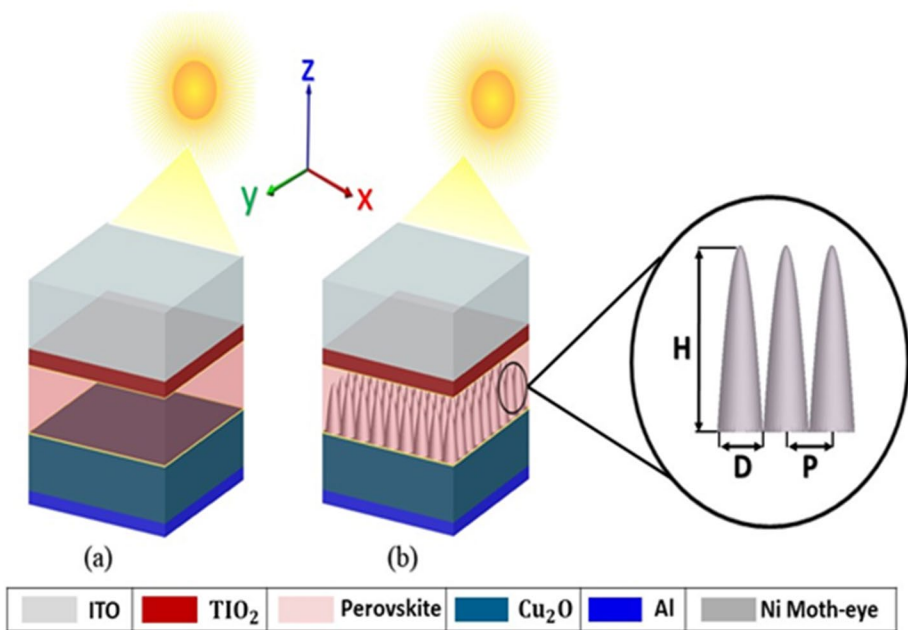


Fig. 1 3D Schematic diagrams of **a** planar PSC and **b** suggested PSC integrated with Ni moth-eye nanostructures

Table 1 Geometrical parameters of the different layers of the PSC

Material	Thickness	References
ITO	500 nm	Baum et al. (2013)
TiO ₂	120 nm	Wang et al. (2013)
MASnI ₃	500 nm	(Roknuzzaman et al. (2018)
Cu ₂ O	420 nm	Nordseth et al. (2017)
Back contact (Al)	100 nm	Palik et al. Palik (1998)
Moth-eye	H	350 nm
	D	165 nm
	P	165 nm

the ITO acts as a PSC contact layer because it has a high conductivity. According to the electrical resistance law, the electrical conductivity increases with the thickness increase, but this will decrease the SC transparency. The TiO₂ layer represents n-type and acts as a buffer layer to avoid charge recombination effect. Therefore, it can be considered as an electron-selective contact layer. The TiO₂ improves the PSCs performance because it is an electron transport material (ETM). Further, active layer of MASnI₃ perovskite material has the ability to molder the bonds and release a large number of electrons because of its high absorption coefficient. It is aimed to improve the conversion efficiency of the proposed PSC, by trapping the light in the perovskite layer to enhance the light absorption. Therefore, moth-eye nanostructures are embedded in the active layer with diameter (D), lattice constant (P) and height (H) as illustrated in Fig. 1b. The nanostructures can enhance the PSC efficiency where localized surface plasmon resonances can be produced to increase the absorption of the active material. The fourth layer of the proposed PSC is Cu₂O which acts as a p-type material. This is due to its low processing solution temperature with high transparency (Bhargava et al. 2018). The holes are collected at the Aluminum back-contact layer. Further, light will be reflected back to the active material by the Al layer which improves the light absorption. To prevent surface oxidation and contamination of the cell, the proposed design PSC is coated with protective material of SiO₂ (Adam et al. 2020; Soliman et al. 2020a, 2020b). The thickness of each layer is illustrated in Table 1.

The absorption of the PSC is calculated using the following equation (Abdel-Latif et al. 2018).

$$A(\lambda) = 1 - R(\lambda) - T(\lambda) \quad (1)$$

where $A(\lambda)$ is the wavelength dependent absorption in the cell, $R(\lambda)$ is the light reflectance, $T(\lambda)$ represents the wavelength dependent transmittance. In this study, the ultimate efficiency (η) of the reported SC is given by Eq. (2) (Huang et al. 2012), assuming no recombination loss. Additionally, every absorbed photon result in the formulation of an electron hole pairs.

$$\eta = \frac{\int_{\lambda_1}^{\lambda_g} F_s(\lambda) * A(\lambda) \frac{\lambda}{\lambda_g} d\lambda}{\int F_s(\lambda) d\lambda} \quad (2)$$

where λ_g is the bandgap wavelength of MASnI₃, $\lambda_{-1} = 300$ nm, and $F_s(\lambda)$ represents the photon flux density at AM1.5 (Spectral and Irradiance: (<http://rredc.nrel.gov/solar/spectra/>

[am/astmg173/astmg173.html](http://am.astmg173/astmg173.html)). The photo current density can be estimated by (Lin et al. 2009):

$$J_{ph} = \eta \frac{e\lambda_g}{hc} \int F_s(\lambda) d\lambda \tag{3}$$

where e is electron charge, c is the light speed, and h is the plank’s constant. The optical electron–hole pair generation rate in the absorber layer is calculated by the following equation (Abdelraouf et al. 2016):

$$G_{opt} = \frac{\epsilon'' E^2}{2h} \tag{4}$$

where G_{opt} is the optical generation rate, E is the electrical field and ϵ is the imaginary part of permittivity.

3 Numerical results and discussion

The simulation is performed by using three-dimensional finite difference time domain (3D—FDTD) based on Lumerical software package to evaluate the light absorption of the suggested design. The sunlight is simulated by a plane source localized above the structure, which has a solar spectral irradiance of AM1.5 through a wide range of wavelength from 300 to 4000 nm. The unit cell of the nanostructured PSC is shown in Fig. 2. Plane wave source in the wavelength range of 200 to 1500 nm is propagated in z-back ward direction. The studied wavelength range is from 300 to 1250 nm. Smallest wavelength of 300 nm is used which is the onset wavelength of solar irradiation. Largest wavelength of 1250 nm is used where $\lambda_g = 1200$ nm for $CH_3NH_3SnI_3$ material. To reduce the computational time,

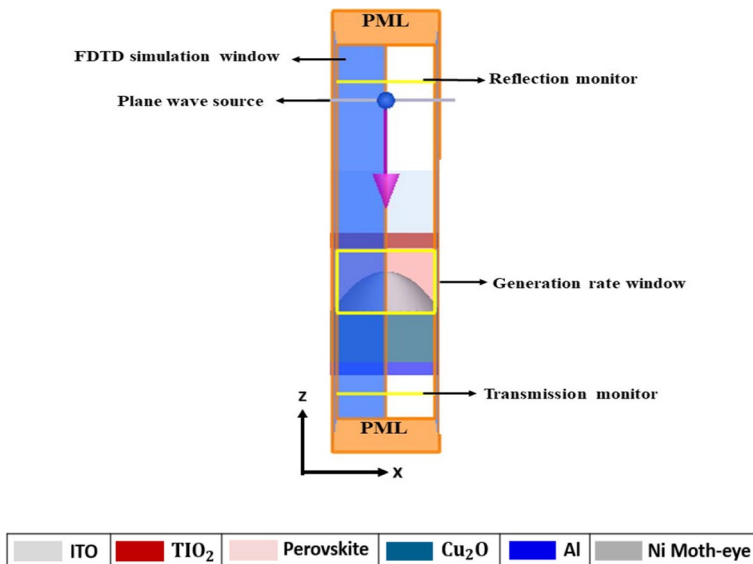


Fig. 2 The x–z plane unit cell of the proposed design

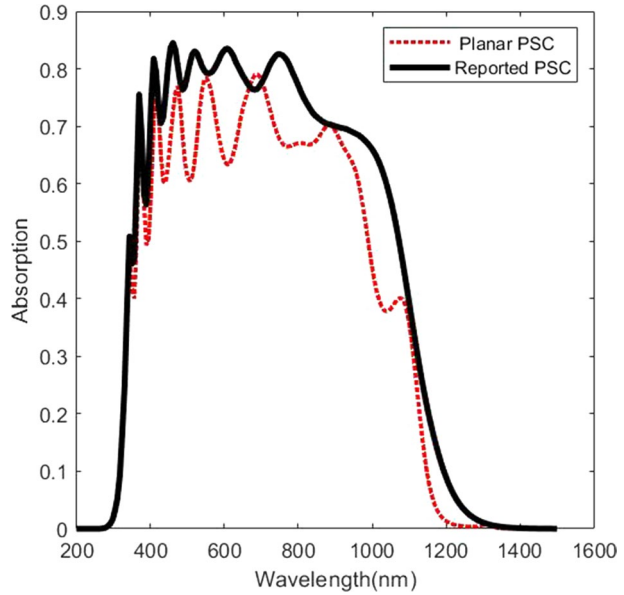
symmetric and asymmetric boundary conditions in X- and Y- directions are used as a replacement of periodic boundary conditions (Khattak et al. 2018). Further, perfectly matched layer (PML) boundary conditions are used in the Z direction. Non-uniform conformal meshing is also used to reduce the meshing errors with high accuracy. In order to obtain accurate results, minimum meshing size of $dx = dy = dz = 1.0$ nm is used. By using frequency-domain power monitors, the transmission and reflection are estimated. In this context, a monitor is placed above the plane wave source as shown in Fig. 2 to calculate the light reflectance $R(\lambda)$. Further, another monitor is placed below the back contact layer to calculate the transmission $T(\lambda)$. Table 2 shows the simulation parameters of the reported SC. The optical constants of ITO/TiO₂/CH₃NH₃SnI₃/Cu₂O are taken from the reported measurements in (Baum et al. 2013; Wang et al. 2013; Roknuzzaman et al. 2018; Nordseth et al. 2017). The back Al and Ni moth-eye nano structure optical constants are selected from Palik's handbook (Palik et al. 1998). Initially, planar PSC illustrated in Fig. 1a is simulated with an optical model to calculate and estimate the absorption, photocurrent density, optical generation rate and the ultimate efficiency. Then, moth-eye nanostructures from Ni material are added to the active layer as shown in Fig. 1b to enhance and maximize the absorption and carrier generation rate. The Ni moth-eye has height H of 350 nm, diameter D of 165 nm and lattice constant P of 165 nm. These dimensions have been selected after doing an optimization to achieve high absorption in the PSC.

Figure 3 shows the absorption curve of the planar and proposed PSCs. It may be seen that there is an increase in the light absorption using the moth-eye nanostructure PSC with improved light trapping. Therefore, there is an increase in the photo current density, generation rate and ultimate efficiency. The moth-eye Ni nanostructures inside the active layer concentrate the electromagnetic field through the active layer with an enhanced near-field

Table 2 The parameters of the FDTD simulation of the suggested PSC

Parameter category	Parameter name	Parameter setting
FDTD simulation Region settings	Mesh accuracy	4
	Mesh type	Auto non-uniform
	Mesh refinement	Conformal variant 1
	PML type	Uniaxial anisotropic PML
	Time step dt stability factor	0.99 (unitless)
	Time step dt	0.0053 fs
	Minimum mesh step	0.25 nm
	Simulation time	1000 fs
Plane wave source settings	Minimum number of layers	32
	Source shape	Plane wave
	Amplitude	1—normalized
	Phase	0
	Polarization angle	0
	Plane wave type	Bloch/periodic
	Time domain pulse type	Broad band
	Time domain frequency	849.41 THz
	Pulse length	1.33 fs
	Offset	3.78 fs
Power monitor settings (transmission and reflection)	Band width	1299.1 THz
	Data recording method	Standard flourier transform
	Monitor type	2D Z-normal
	Partial spectral averaging Δ	10 THz
	Spatial interpolation method	Nearest mesh cell

Fig. 3 Absorption spectra of the planar PSC and moth-eye based PSC



scattering in the vicinity of the structure. Figure 4b shows the electric field profile of the moth-eye structure PSC at a wavelength of 750 nm compared to planar PSC electric field profile in Fig. 4a. It should be noted that the calculated absorption does not contain the absorption of the plasmonic moth-eye nanostructures. It may be seen from these figures that the concentration of electric field of the proposed design PSC is higher than that of the planar SC.

The resonances around the moth-eye nanostructures are due to the supported localized surface plasmons modes. The charge carriers in the nanostructures are vibrated collectively due to the incident of electromagnetic radiation. Since plasmonic nanostructures became close to each other, their near electric fields are overlapped. Therefore, there is an interaction between the electrical fields of these nanostructures. This

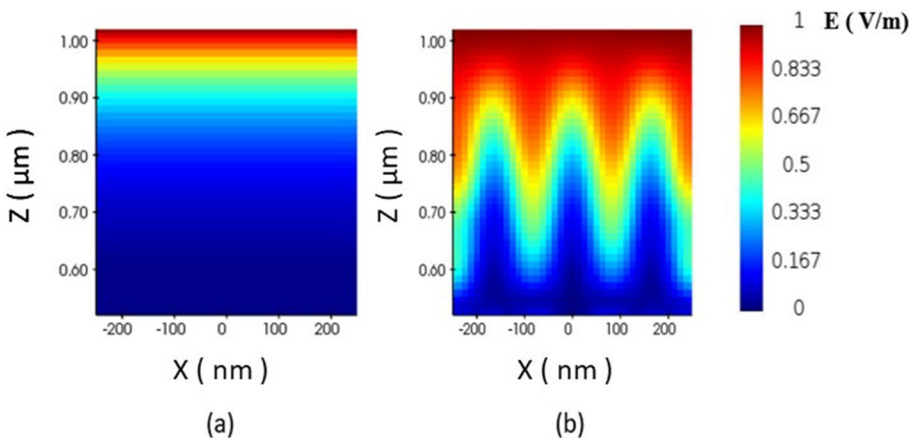


Fig. 4 Electric field profile for **a** planar and **b** moth-eye based PSCs at $\lambda = 750$ nm

leads to new plasmonic modes with different energies than the individual nanostructure. Therefore, an absorption enhancement occurs compared to planar PSC. It means that an improvement in the electric field profile of the cell due to the presence of moth-eye nanostructure in the active layer of perovskite solar cell. Figure 5 shows the optical generation rate profile for the planar and proposed PSCs with moth-eye nanostructures at wavelength of 750 nm. It may be seen that the optical generation rate of the PSC with moth-eye nanostructure is improved as shown in Fig. 5b. The absence of moth-eye nanostructure in the active layer requires more holes to travel a long distance to reach the HTL. This will increase the probability of recombination in the PSC and the transfer of carriers doesn't occur properly. On the other hand, the implemented nanostructures in the active layer help the holes travel over a shorter path than that of the conventional planar PSC. The maximum optical generation rate (G_{opt}) of each structure is estimated using Eq. (4) which is equal to $2.07 \times 10^{28} \text{ (m}^{-3} \cdot \text{s}^{-1}\text{)}$ for the planar and $5.45 \times 10^{28} \text{ (m}^{-3} \cdot \text{s}^{-1}\text{)}$ for the proposed PSC. The photocurrent density (J_{ph}) is also evaluated using Eq. (3) to show the difference between the planar and proposed PSC. The photocurrent density is 44.16 mA/cm^2 for the planar PSC and 46.59 mA/cm^2 for the reported PSC. The ultimate efficiency of the planar and proposed design PSC are 29.29% and 33.81%, respectively.

It's found that the use of moth-eye nanostructure in the active layer increases the efficiency with an enhancement factor of 15.43% than the planar design. Figure 6 shows the ultimate efficiency related to hole transport layer material type. The effect of the material type of the hole transport layer (HTL) is studied with the same thickness of 420. It is shown from the Fig. 6 that the Cu_2O as a hole transport layer introduces the best performance with an ultimate efficiency of 29.29% compared to other materials such as NiO (Souri et al. 2009) of 29.01%, Spiro-OMeTAD (Fantacci et al. 2011) of 28.87%, CuSCN (Pattanasattayavong et al. 2013) of 28.45% and PEDOT: PSS (Fung et al. 2011) 27.92% respectively. Best performance of PSC is achieved with Cu_2O as HTL compared to other studied materials. This is because of the high mobility and conductivity of the copper based inorganic p-type semiconductor material. Further, the Cu_2O has higher valence band than the other materials which is in good alignment with active layer material.

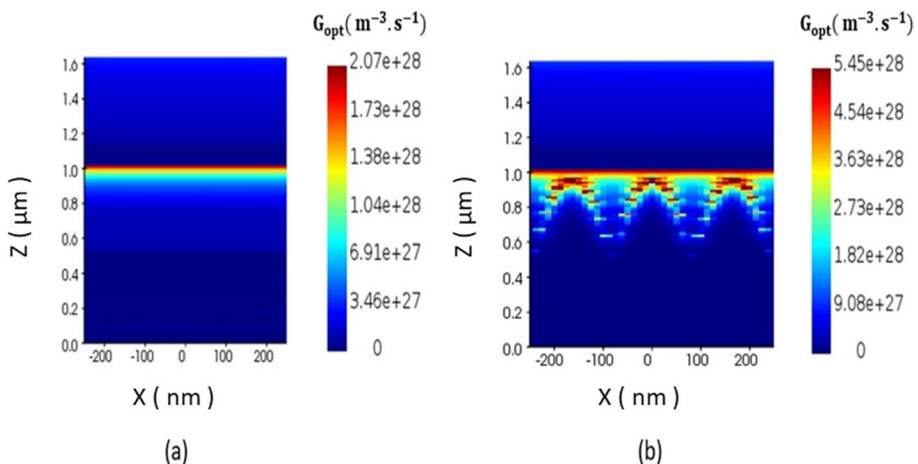
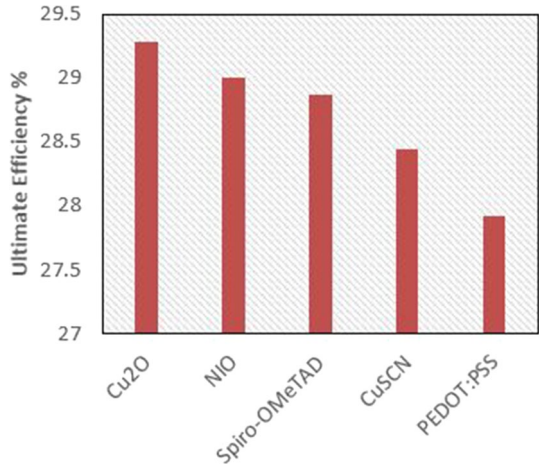


Fig. 5 Optical Generation rate profile for **a** planar **b** moth-eye based PSCs at wavelength of 750 nm

Fig. 6 Impact of the hole transport layer material type on the ultimate efficiency of the reported PSC



In order to choose the perfect electron transport layer (ETL), different types of materials are tested. As shown in Fig. 7, it is evident that the TiO₂ as an electron transport layer achieves the optimum performance with ultimate efficiency of 29.29% compared to other used materials such as SnO₂ (Diana et al. 2010) of 27.6%, PCBM (Lee et al. 2010) of 22.68%, ZnO (Djurišić et al. 2006) of 29.11% and C6O (Dresselhaus et al. 1996) of 25.29%. Best performance of PSC is achieved with TiO₂ as ETL compared to other ETLs. This is because TiO₂ has an appropriate band gap level for electrons injection. The TiO₂ has a better chemical stability, high electron mobility, low installation cost and environmental familiarity as well. TiO₂ material has a suitable bandgap between detractor the transportation of holes.

Nanostructure shape also has a great effect on the ultimate efficiency of the PSC as shown in Fig. 8. It may be seen that the PSC with moth-eye nanostructures achieves higher ultimate efficiency than other nanostructures shown in Table 3. Table 3 shows the different nanostructure shapes integrated in the active layer in this study with their dimensions. It is worth noting that the dimensions of all shapes embedded to the active layer have the same volume. The moth-eye nanostructures-based PSC achieve higher efficiency of 33.81% compared to other shapes such as star, cylindrical and pyramids with efficiencies of 32.53%, 31.8% and 32.6%, respectively. Also, the type of used

Fig. 7 Impact of the electron transport layer material type on the ultimate efficiency of the reported PSC

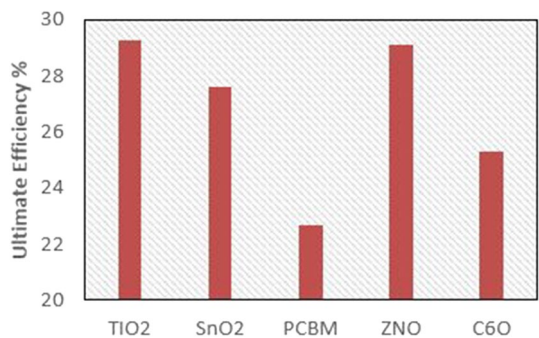


Fig. 8 Impact of the shape of the nanostructure embedded in the active layer on the ultimate efficiency of the reported PSC

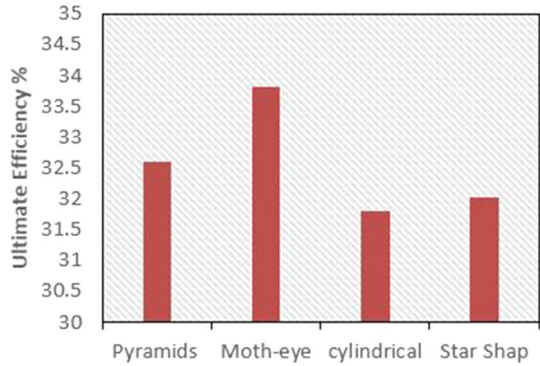

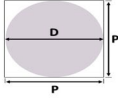

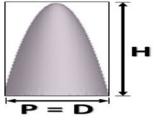

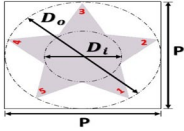

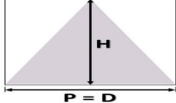


Table 3 Dimensions of different nanostructure shapes

Geometry	Dimensions (nm)		Shape of nanostructure
 Cylinder	P	165	
	D	165	
	H	350	
 Moth-eye	P	165	
	D	165	
	H	350	
 Star shape	P	165	
	D_r	80	
	D_o	165	
	H	350	
	N	5	
 Pyramids	P	165	
	D	165	
	H	350	

material of moth-eye nanostructure is studied to maximize the efficiency of the cell. It is evident from Fig. 9 that the Ni material has achieved better efficiency with an ultimate efficiency of 33.81% compared to other used materials such as Al of 33.36%, Au of 33.56%, Ag of 33.6%, TiO₂ (the same material of ETL) of 30.77%, Cu₂O (the same material of HTL) of 30.79% and GeSe (Eymard et al. 1977) of 33.46%.

It is worth noting that the absorption shown in Fig. 3 includes the absorption of the plasmonic moth eye nanostructures. Therefore, the location of the plasmonic nanostructures above the active layer is tested as shown in the unit cell presented in Fig. 10. The absorption spectra of the proposed design and planar PSCs are shown in Fig. 11. In this study, the geometrical parameters are taken as hole pitch of 500 nm, diameter of

Fig. 9 Impact of the of different nanostructures material on the ultimate efficiency of the reported PSC

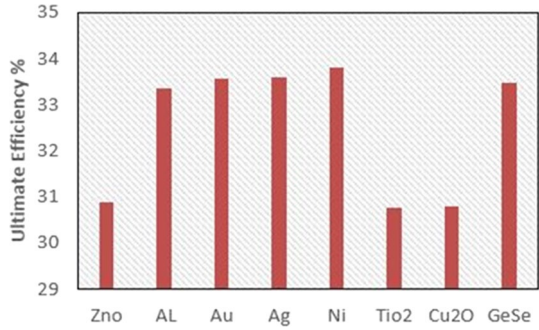


Fig. 10 The unit cell of the proposed design covered by the moth eye nanostructures in the x-z plane

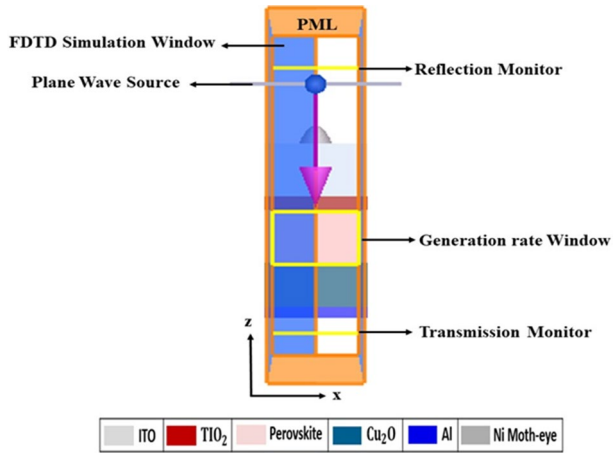
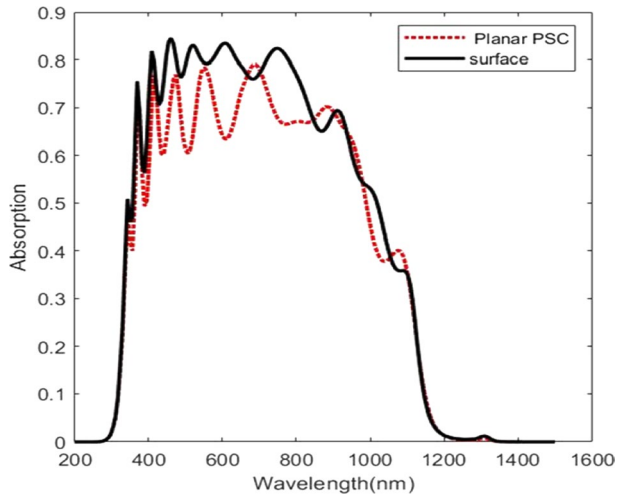


Fig. 11 Absorption spectra of the planar PSC and PSC covered by moth-eye nanostructures



50 nm and height of 350 nm. It is evident that the absorption spectra of the moth-eye nanostructure PSC's enhanced the light trapping and increased light absorption. Consequently, the generation rate, the photo current density, and the overall efficiency all

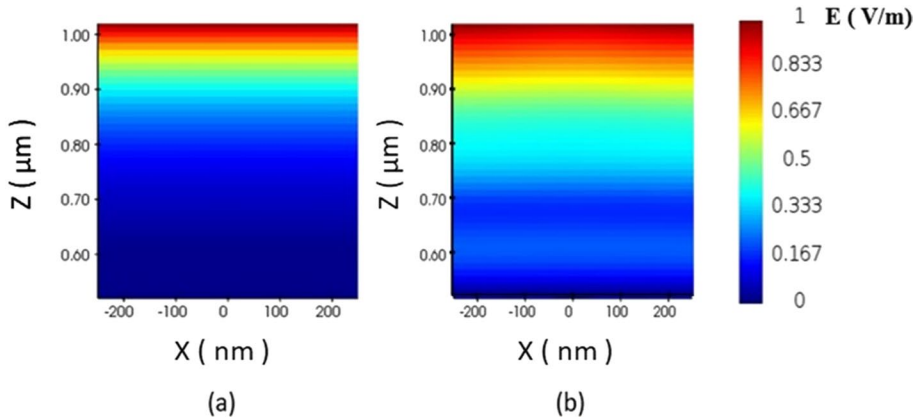


Fig. 12 Electric field profile through the active layer of the **a** planar and **b** PSCs covered by the moth-eye nanostructures at $\lambda = 750$ nm

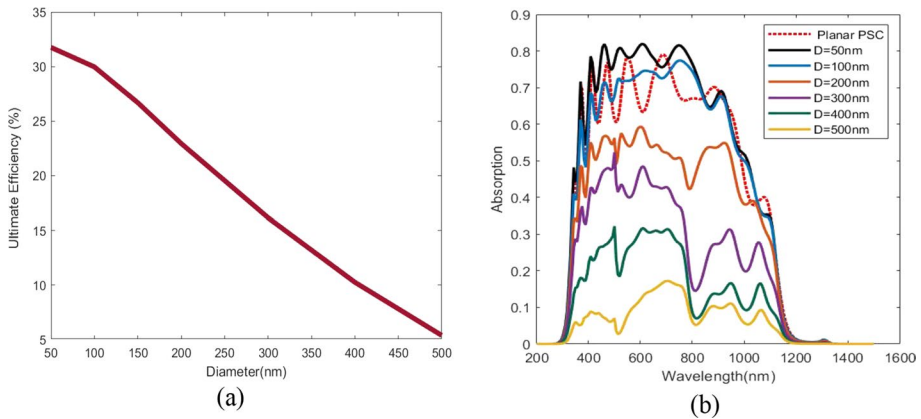


Fig. 13 Impact of the moth-eye diameter on **a** the ultimate efficiency **b** the absorption of reported PSC

increase. The moth-eye Ni nanostructures on surface focus the electromagnetic field with enhanced near-field scattering around the nanostructure structure. Figure 12 shows the electric field profile through the active layer of the planar and PSCs covered by the moth-eye nanostructures at $\lambda = 750$ nm. It may be seen that the proposed design has better electric field concentration and hence greater generation rate in the active layer compared to that of the planar SC. The PSC with moth-eye nanostructure on the surface has an enhanced optical generation rate of $3.38 \text{ e}^{28} \text{ (m}^{-3} \cdot \text{s}^{-1}\text{)}$ than planar SC of $2.07 \text{ e}^{28} \text{ (m}^{-3} \cdot \text{s}^{-1}\text{)}$. Equation (3) is used to evaluate the photocurrent density (J_{ph}) in order to demonstrate the differences between the surface proposed PSC and the planar PSC. The photocurrent density for the reported PSC is equal to 46.0082 mA/cm^2 , whereas it is 44.16 mA/cm^2 for the planar PSC. The planar PSC’s overall efficiency is 29.29% whereas the reported PSC with moth-eye nanostructures is 31.76%.

The diameter of the moth-eye nanostructures over the PSC is also investigated at a constant hole pitch of 500 nm. Figure 13 shows the ultimate efficiency and absorption

variations with the moth-eye diameter. It is evident that the absorption and hence the ultimate efficiency decrease by increasing the plasmonic nanostructure diameter. The large diameter prevents the light penetration through the active material of the PSC with large reflection. Maximum ultimate efficiency of 31.76% is obtained at a diameter of 50 nm. Table 4 shows a comparison between the reported nanostructured PSC and those reported in the literature. It is evident that the suggested PSC covered by plasmonic moth-eye nanostructures achieve higher photocurrent density than those suggested in the literature (Patel 2021a, b, Jayan et al. 2021, Qasim et al. 2021, Alam et al. 2020, Sunny et al. 2021).

4 Fabrication methodology

The 3rd generation perovskite solar cell fabrication is simple. It requires less energy compared to silicon solar cells. The temperature required for fabrication process is about 450 °C which is low compared to temperature of 1200 °C required for silicon. Figure 14 shows the fabrication steps of PSC. First, Indium tin oxide (ITO) is cleaned with several materials such as ethanol, acetone, isopropanol, and deionized water respectively. Then, ITO is electrolyzed in FeCl₃ solution to etch the ITO (<https://www.ossila.com/collections/substrates-and-fabrication>). A compact layer (TiO₂) is next treated carefully using the aqueous solution of TiCl₄ which is used to dip the film for 30 min at about 70 °C, rinsed with deionized water and annealed at 450 °C for 30 min. Then, the TiO₂ is cooled to temperature room. Finally, a compact layer (TiO₂) is deposited on the ITO substrate by spin coating for 30 s at 3000 rpm (this step will be repeated twice followed by annealing at 145 °C for 15 min for each time) (Cojocaru et al. 2015). The next step, perovskite films are prepared by spin coating as follows, The SnI₂ will be spin coated at 3000 rpm for 30 s on TiO₂ by dipping it in N, N-dimethyl formamide (DMF) where small amount of BTA will be added to the solution. Then, it will be annealed at 70 °C for about 15 min and will be cooled to the room temperature. The methylammonium (MA) iodide solution will be next spin coated at 4000 rpm at 45 s onto SnI₂ films after dipping in solution. Finally, the samples will be annealed at 145 °C for about 30 min to grow into MASnI₃ films (<https://www.ossila.com/collections/substrates-and-fabrication>; Bi et al. 2014).

To add nanostructure of Ni in the perovskite layer, thermal deposition can be used at about 450 °C followed by annealing process at 145 °C. Then, it will be cooled to room temperature. The perovskite layer active layer with Ni nanostructure is now ready to be active layer in the PSC (Saliba et al. 2018). Now spin coat a solution of Cu₂O on top of the

Table 4 Comparison between the reported nanostructured PSC and those reported in the literature

Device architecture	(J_{ph}) mA/cm ²	Year	Ref
Planar ITO/TiO ₂ /MASnI ₃ /Cu ₂ O/AL	44.16	This study	
Proposed PSC design. Ni/ITO/TiO ₂ /MASnI ₃ /Cu ₂ O/AL	46.0082		
FTO/TiO ₂ /MASnI ₃ /Cu ₂ O/Anode	40.14	Feb 2021	Patel (2021a, b)
FTO/PCBM/MASnI ₃ /CuI/Au	34.27	March 2021	Jayan et al. (2021)
FTO/ZnO/CdS/MASnI ₃ /GaAs/Au	33.86	Nov2021	Qasim et al. (2021)
FTO/In ₂ S ₃ /MASnI ₃ /Spiro-OMeTAD/Au	33.44	Dec 2020	Alam et al. (2020)
FTO/TiO ₂ /MASnI ₃ /Ni	31.93	June 2021	Sunny et al. (2021)

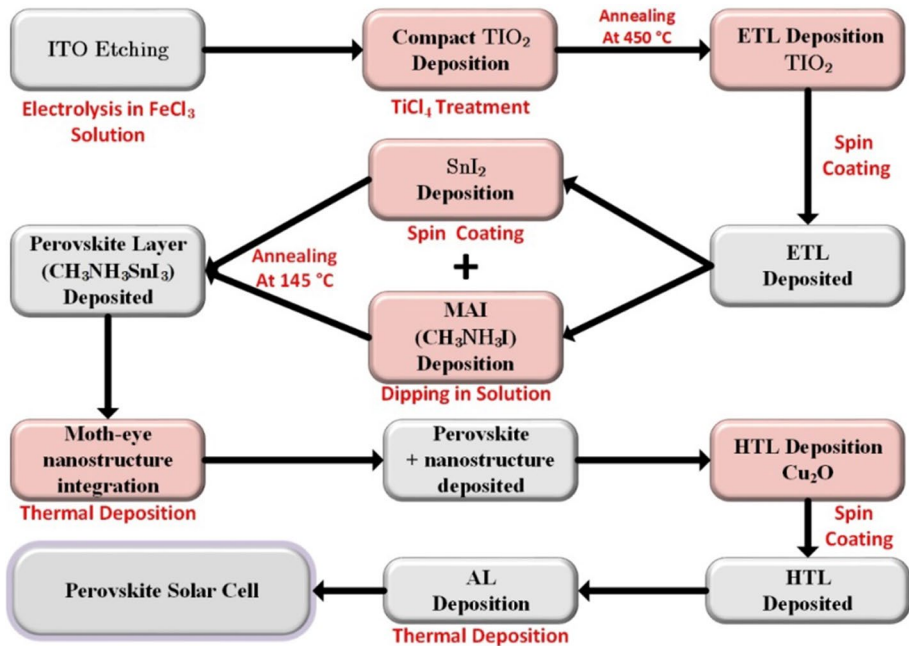


Fig. 14 Flow diagram of PSC fabrication process

perovskite layer at 2000 rpm for about 45 s to form the Cu₂O film. After spin coat process, we will leave it in a desiccator overnight in air. This allows the Cu oxidation which will further p-dope the Cu₂O making it more conductive for holes. Before evaporating the AL metal contact using thermal deposition (Liu et al. 2013), we can remove the excess material around the active area with a razor (<https://www.ossila.com/collections/substrates-and-fabrication>). The PSC is now ready to be used for converting sunlight into electrical power. Regarding the second design, the Ni nanostructures can be deposited over the PSC surface using thermal deposition at 450 °C. Then, an annealing process can be done at 145 °C and cooled at room temperature on the ITO layer (Saliba et al. 2018).

5 Conclusion

Lead -free MASnI₃ based PSC performance is studied and analyzed to maximize the light absorption using FDTD simulation based on Lumerical package software. It is found that the suggested PSC integrated with Ni moth-eye nanostructures achieves better light absorption than other nanostructures. The numerical results show that the planar PSC has a photocurrent density of 44.16 mA/cm², an optical generation rate of 2.07 e28 (m⁻³. s⁻¹) and an ultimate efficiency of 29.29%. The integration of moth-eye nanostructure in the proposed design PSC improves and enhances the light absorption in the cell due to the excitation of localized surface plasmon resonances above the surface. The proposed PSC achieves photocurrent density of 46.0082 mA/cm² with an enhancement of 5.43% relative to planar PSC. Further, an optical generation rate 3.38 e²⁸ (m⁻³. s⁻¹) and an ultimate efficiency of

31.76% are obtained with an improvement of 63.29% and 14.496% relative to planar PSC at AM1.5 global condition.

Author contribution GYA-L and MFOH, have proposed the idea. ASW has done the simulations of the reported PSC. All authors have contributed to the analysis, discussion, writing and revision of the paper.

Funding Open access funding provided by The Science, Technology & Innovation Funding Authority (STDF) in cooperation with The Egyptian Knowledge Bank (EKB). The authors acknowledge the financial support received from the Academy of Scientific Research and Technology (ASRT) at Egypt under the South Africa-Egypt Cooperation.

Data availability The data will be available upon request.

Declarations

Conflict of interest The authors would like to clarify that there are no financial/non-financial interests that are directly or indirectly related to the work submitted for publication.

Ethical approval The authors declare that there are no conflicts of interest related to this article.

Open Access This article is licensed under a Creative Commons Attribution 4.0 International License, which permits use, sharing, adaptation, distribution and reproduction in any medium or format, as long as you give appropriate credit to the original author(s) and the source, provide a link to the Creative Commons licence, and indicate if changes were made. The images or other third party material in this article are included in the article's Creative Commons licence, unless indicated otherwise in a credit line to the material. If material is not included in the article's Creative Commons licence and your intended use is not permitted by statutory regulation or exceeds the permitted use, you will need to obtain permission directly from the copyright holder. To view a copy of this licence, visit <http://creativecommons.org/licenses/by/4.0/>.

References

- Abdel-Latif, G.Y., Hameed, M.F.O., Hussein, M., Abdel-Razzak, M., Obayya, S.S.A.: Characteristics of highly efficient star-shaped nanowires solar cell. *J. Photonics Energy* **8**(4), 047001–047015 (2018). <https://doi.org/10.1117/1.JPE.8.047001>
- Abdelraouf, O.A.M., Allam, N.K.: Towards nanostructured perovskite solar cells with enhanced efficiency: coupled optical and electrical modeling. *Sol. Energy* **137**, 364–370 (2016)
- Adam, S.A., et al.: Effect of temperature on the stability and optical properties of SiO₂-water nanofluids for hybrid photovoltaic/thermal applications. *Appl. Therm. Eng.* **175**, 115394–115405 (2020)
- Alam, I., Ashraf, M.A.: Effect of different device parameters on tin-based perovskite solar cell coupled with In₂S₃ electron transport layer and CuSCN and Spiro-OMeTAD [25] alternative hole transport layers for high-efficiency performance. *Mater. Sci.* 1–17 (2020). <https://doi.org/10.1080/15567036.2020.1820628>
- Baum, M., Alexeev, I., Latzel, M., Christiansen, S.H., Schmidt, M.: Determination of the effective refractive index of nanoparticulate ITO layers. *Opt. Express* **21**, 22754–22761 (2013)
- Bhargava, R., Khan, S.: Enhanced optical properties of Cu₂O anchored on reduced graphene oxide (rGO) sheets. *J. Phys. Condens. Matter* **30**(33), 335703–335736 (2018)
- Bi, D., El-Zohry, A.M., Hagfeldt, A., Boschloo, G.: Improved morphology control using a modified two-step method for efficient PSCs. *ACS Appl. Mater. Interfaces* **6**, 18751–18757 (2014). <https://doi.org/10.1021/am504320h>
- Burschka, J., et al.: Sequential deposition as a route to high-performance perovskite-sensitized solar cells. *Nature* **499**, 316–319 (2013)
- Chen, Y., et al.: Improved optical properties of perovskite solar cells by introducing Ag nanoparticles and ITO AR layers. *Sci. Rep.* **11**(1), 14550–14559 (2021)
- Cojocar, L., Uchida, S., Sanehira, Y., Nakazaki, J., Kubo, T., Segawa, H.: Surface treatment of the compact TiO₂ layer for efficient planar heterojunction PSCs. *Chem. Lett.* **44**, 674–676 (2015). <https://doi.org/10.1246/cl.150068>

- Diana, T., Nomita, D.K., Sarma, H.: On the optical properties of SnO₂ thin films prepared by sol-gel method. *Indian J. Phys.* **84**, 687–691 (2010). <https://doi.org/10.1007/s12648-010-0072-5>
- Djurišić, A.B., Leung, Y.H.: Optical properties of ZnO nanostructures. *Small* **2**(8–9), 944–961 (2006)
- Dresselhaus, M.S., et al.: Optical properties of C60 and related materials. *Synth. Met.* **78**(3), 313–325 (1996)
- Eymard, R., Otto, A.: Optical and electron-energy-loss spectroscopy of GeS, GeSe, SnS, and SnSe single crystals. *Phys. Rev. B* **16**, 1616–1623 (1977)
- Fantacci, S., et al.: Electronic and optical properties of the spiro-MeOTAD hole conductor in its neutral and oxidized forms: a DFT/TDDFT investigation. *J. Phys. Chem. C* **115**(46), 23126–23133 (2011)
- Fung, D.D.S., et al.: Optical and electrical properties of efficiency enhanced polymer solar cells with Au nanoparticles in a PEDOT–PSS layer. *J. Mater. Chem.* **21**(41), 16349–16356 (2011)
- Guo, Y., et al.: Effects of transition metal substituents on interfacial and electronic structure of CH₃NH₃PbI₃/TiO₂ interface: a first-principles comparative study. *Nanomaterials* **9**, 966–979 (2019)
- Hao, F., Stoumpos, C.C., Cao, D.H., Chang, R.P.H., Kanatzidis, M.G.: Lead-free solid-state organic-inorganic halide perovskite solar cells. *Nat. Photonics* **8**, 489–494 (2014a)
- Hao, F., Stoumpos, C.C., Cao, D.H., Chang, R.P.H., Kanatzidis, M.G.: Lead-free solid-state organic-inorganic halide perovskite solar cells. *Nat. Photonics* **8**(6), 489–494 (2014b). <https://doi.org/10.1038/nphoton.2014.82>
- Heidarzadeh, H., Tavousi, A.: Design of an LSPR-enhanced ultrathin CH₃NH₃PbX₃ perovskite solar cell incorporating double and triple coupled nanoparticles. *J. Electron. Mater.* **50**(4), 1817–1826 (2021) <https://www.lumerical.com/> <https://www.ossila.com/collections/substrates-and-fabrication>
- Huang, N., Lin, C., Povinelli, M.L.: Broadband absorption of semiconductor nanowire arrays for photovoltaic applications. *J. Opt.* **14**(2), 024004 (2012)
- Huang, H.H., Shih, Y.C., Wang, L., Lin, K.F.: Boosting the ultra-stable unencapsulated perovskite solar cells by using montmorillonite/CH₃NH₃PbI₃ nanocomposite as photoactive layer. *Energy Environ. Sci.* **12**, 1265–1273 (2019)
- Hwang, T., Cho, D., Kim, J., et al.: Investigation of chlorine mediated microstructural evolution of CH₃NH₃PbI₃(Cl) grains for high optoelectronic responses. *Nano Energy* **25**, 91–99 (2016). <https://doi.org/10.1016/j.nanoen.2016.04.044>
- Izadi, F., Ghobadi, A., Gharaati, A., Minbashi, M., Hajjiah, A.: Effect of interface defects on high efficient perovskite solar cells. *Optik* **227**, 166061–166069 (2021)
- Jayan, K.D., Sebastian, V.: Comprehensive device modelling and performance analysis of MASnI₃ based perovskite solar cells with diverse ETM, HTM and back metal contacts. *Sol. Energy* **217**, 40–48 (2021)
- Jeong, J., Kim, M., Seo, J., Lu, H., Ahlawat, P., Mishra, A., et al.: Pseudo-halide anion engineering for α -FAPbI₃ perovskite solar cells. *Nature* **592**(7854), 381–385 (2021). <https://doi.org/10.1038/s41586-021-03406-5>. PMID:33820983
- Jiang, X., Li, H., Zhou, Q., Wei, Q., Wei, M., Jiang, L., et al.: One-step synthesis of SnI₂·(DMSO)_x adducts for high-performance tin perovskite solar cells. *J. Am. Chem. Soc.* **143**(29), 10970–10976 (2021). <https://doi.org/10.1021/jacs.1c03032>. PMID:34196528
- Khaled, A., et al.: Modeling and characteristics of a nanostructured NiO/GeSe core-shell perovskite solar cell. *JOSA B* **38**(11), 3441–3447 (2021)
- Khattak, Y.H., et al.: Effect of Cu₂O hole transport layer and improved minority carrier lifetime on the efficiency enhancement of Cu₂NiSnS₄ based experimental solar cell. *J. Renew. Sustain. Energy* **10**, 043502–043513 (2018)
- Lee, W.H., et al.: Exploiting optical properties of P3HT: PCBM films for organic solar cells with semi-transparent anode. *Thin Solid Films* **518**(24), 7450–7454 (2010)
- Lin, C., Povinelli, M.L.: Optical absorption enhancement in silicon nanowire arrays with a large lattice constant for photovoltaic applications. *Opt. Express* **17**(22), 19371–19381 (2009)
- Liu, M., Johnston, M.B., Snaith, H.J.: Efficient planar heterojunction PSCs by vapor deposition. *Nature* **501**, 395–398 (2013). <https://doi.org/10.1038/nature12509>
- Liu, J., Yao, M., Shen, L.: Third generation photovoltaic cells based on photonic crystals. *J. Mater. Chem. C* **7**(11), 3121–3145 (2019a)
- Liu, D., Li, Q., Hu, J., Jing, H., Wu, K.: Predicted photovoltaic performance of lead-based hybrid perovskites under the influence of a mixed-cation approach: theoretical insights. *J. Mater. Chem. C* **7**, 371–379 (2019b)
- Moerland, R.J., et al.: Subnanometer-accuracy optical distance ruler based on fluorescence quenching by transparent conductors. *Optica* **3**, 112–117 (2016)
- National Renewable Energy Laboratory: Photovoltaic research (2021). <https://www.nrel.gov/pv/>

- Noel, N.K., Stranks, S.D., Abate, A., Wehrenfennig, C., Guarnera, S., Haghighirad, A.-A., et al.: Lead-free organic-inorganic tin halideperovskites for photovoltaic applications. *Energy Environ. Sci.* **7**(9), 3061–3068 (2014). <https://doi.org/10.1039/C4EE01076K>
- Nordseth, Ø., et al.: Optical analysis of a ZnO/Cu₂O subcell in a silicon-based tandem heterojunction solar cell. *Green Sustain. Chem.* **7**(1), 57–69 (2017)
- Noof, R., Zweibel, K.: High-efficiency CdTe and CIGS thinfilm solar cells: highlights and challenges. In: Conference Record of the 2006 IEEE 4th World Conference on Photovoltaic Energy Conversion, WCPEC-4. pp. 317–320, IEEE (2007)
- Palik, E.D.: Handbook of Optical Constants of Solids. Academic Press, Cambridge (1998)
- Park, N.-G., Miyasaka, T., Grätzel, M.: Organic-Inorganic Halide Perovskite Photovoltaics. Springer, Cham (2016)
- Patel, P.K.: Device simulation of highly efficient eco-friendly CH₃NH₃SnI₃ perovskite solar cell. *Sci. Rep.* **11**, 3082–3093 (2021a). <https://doi.org/10.1038/s41598-021-82817-w>
- Patel, P.K.: Device simulation of highly efficient eco-friendly CH₃NH₃SnI₃ perovskite solar cell. *Sci. Rep.* **11**(1), 1–11 (2021b)
- Pattanasattayavong, P., Ndjawa, G.O.N., Zhao, K., Chou, K.W., Yaacobi-Gross, N., O'Regan, B.C., Amassian, A., Anthopoulos, T.D.: Electric field-induced hole transport in copper (I) thiocyanate (CuSCN) thin-films processed from solution at room temperature. *Chem. Commun.* **49**, 4154–4156 (2013)
- Poortmans, J., Arkhipov, V.: Thin Film Solar Cells: Fabrication, Characterization and Applications (Wiley Series in Materials for Electronic & Optoelectronic Applications). Wiley, New York (2006)
- Qasim, I., Ahmad, O., Rashid, A., Zehra, T., Malik, M., Rashid, M., Ahmed, M.W., Nasir, M.: Numerical optimization of (FTO/ZnO/CdS/CH₃NH₃SnI₃/GaAs/Au) perovskite solar cell using solar capacitance simulator with efficiency above 23% predicted. *Opt. Quantum Electron.* **53**, 456–474 (2021). <https://doi.org/10.1007/s11082-021-03361-5>
- Roknuzzaman, M., et al.: Insight into lead-free organic-inorganic hybrid perovskites for photovoltaics and optoelectronics: a firstprinciples study. *Org. Electron.* **59**, 99–106 (2018)
- Saffari, M., et al.: DFT analysis and FDTD simulation of CH₃NH₃PbI₃-xCl_x mixed halide perovskite solar cells: role of halide mixing and light trapping technique. *J. Phys. D Appl. Phys.* **50**(41), 415501–4155177 (2017)
- Saliba, M., Correa-Baena, J.-P., Grätzel, M., Hagfeldt, A., Abate, A.: Perovskite solar cells: from the atomic level to film quality and device performance. *Angew. Chem. Int. Ed.* **57**, 2554–2569 (2018). <https://doi.org/10.1002/anie.201703226>
- Soliman, T.S., Vshivkov, S.A., Elkalashy, S.I.: Structural, linear and nonlinear optical properties of Ni nanoparticles–Polyvinyl alcohol nanocomposite films for optoelectronic applications. *Opt. Mater.* **107**, 110037–110047 (2020a)
- Soliman, T.S., Vshivkov, S.A., Elkalashy, S.I.: Structural, thermal, and linear optical properties of SiO₂ nanoparticles dispersed in polyvinyl alcohol nanocomposite films. *Polym. Compos.* **41**(8), 3340–3350 (2020b)
- Souri, D., Salehizadeh, S.A.: Effect of NiO content on the optical band gap, refractive index, and density of TeO₂-V₂O₅-NiO glasses. *J. Mater. Sci.* **44**, 5800–5805 (2009)
- Solar Spectral Irradiance: ASTM G-173, standard tables for reference solar spectral irradiances: direct normal and circumsolar. National Renewable Energy Laboratory. <http://rredc.nrel.gov/solar/spectra/am/astmg173/astmg173.html>
- Sunny, A., et al.: Numerical study of high performance HTL-free CH₃NH₃SnI₃-based perovskite solar cell by SCAPS-1D. *AIP Adv.* **11**(6), 065102–065112 (2021)
- Umari, P., et al.: Relativistic GW calculations on CH₃NH₃PbI₃ and CH₃NH₃SnI₃ perovskites for solar cell applications. *Sci. Rep.* **4**, 4467–4474 (2014)
- Wang, X., Wu, G., Zhou, B., Shen, J.: Optical constants of crystallized TiO₂ coatings prepared by sol-gel process. *Materials* **6**, 2819–2830 (2013)
- Yan, J., Saunders, B.R.: Third-generation solar cells: a review and comparison of polymer: fullerene, hybrid polymer and perovskite solar cells. *Rsc Adv.* **4**(82), 43286–43314 (2014)
- Yu, W., et al.: Ultrathin Cu₂O as an efficient inorganic hole transporting material for perovskite solar cells. *Nanoscale* **00**, 1–7 (2015)